The Cryosphere Discuss., 8, 5137–5168, 2014
www.the-cryosphere-discuss.net/8/5137/2014/
doi:10.5194/tcd-8-5137-2014

The Cryosphere Discussions
Open Access

Geophysical mapping of palsa peatland permafrost

Y. Sjöberg[1], P. Marklund[2], R. Pettersson[2], and S. W. Lyon[1]

[1]Stockholm University, Stockholm, Sweden
[2]Uppsala University, Uppsala, Sweden

Received: 15 August 2014 – Accepted: 23 September 2014 – Published: 13 October 2014

Correspondence to: Y. Sjöberg (ylva.sjoberg@natgeo.su.se)

Published by Copernicus Publications on behalf of the European Geosciences Union.

Abstract

Permafrost peatlands are hydrological and biogeochemical hotspots in the discontinuous permafrost zone. Non-intrusive geophysical methods offer possibility to map current permafrost spatial distributions in these environments. In this study, we estimate the depths to the permafrost table surface and base across a peatland in northern Sweden, using ground penetrating radar and electrical resistivity tomography. Seasonal thaw frost tables (at ~0.5 m depth), taliks (2.1–6.7 m deep), and the permafrost base (at ~16 m depth) could be detected. Higher occurrences of taliks were discovered at locations with a lower relative height of permafrost landforms indicative of lower ground ice content at these locations. These results highlight the added value of combining geophysical techniques for assessing spatial distribution of permafrost within the rapidly changing sporadic permafrost zone. For example, based on a simple thought experiment for the site considered here, we estimated that the thickest permafrost could thaw out completely within the next two centuries. There is a clear need, thus, to benchmark current permafrost distributions and characteristics particularly in under studied regions of the pan-arctic.

1 Introduction

Permafrost peatlands are widespread across the Arctic and cover approximately 12 % of the arctic permafrost zone (Hugelius et al., 2013, 2014). They often occur in areas climatically marginal to permafrost due to the thermal properties of peat. In the sporadic permafrost zone the ground temperature in these peatlands is often close to 0 °C, and therefore sensitive to fluctuations in climate. Permafrost distribution and thawing in these landscapes is influenced by several factors other than climate, including hydrological, geological, morphological and erosional processes, that often combine in complex interactions (e.g., McKenzie and Voss, 2013; Painter et al., 2013; Zuidhoff, 2002). Due to complex interactions between these factors these peatlands are often

TCD
8, 5137–5168, 2014

dynamic with regards to their permafrost structures and extent as the distribution of permafrost landforms (such as dome shaped palsas and flat-topped peat plateaus) and talik landforms (such as hollows, fens and lakes) vary with climatic and local conditions (e.g., Sannel and Kuhry, 2011; Seppälä 2011; Wramner, 1968). This dynamic nature and variable spatial extent has potential implications across the pan-Arctic as these permafrost peatlands store large amounts of soil organic carbon (Hugelius et al., 2014; Tarnocai et al., 2009). The combination of large carbon storage and high potential for thawing make permafrost peatlands biogeochemical hotspots in the warming Arctic. In light of this, predictions of future changes in these environments require knowledge of current permafrost distributions and characteristics, which is sparse in today's scientific literature.

While most observations of permafrost and its condition across the landscape to-date consist of temperature measurements from boreholes, advances in geophysical methods provide a good complement for mapping the permafrost distribution in space. Such techniques can provide information about permafrost thickness and the extents and distribution of taliks, which can usually not be obtained from borehole data alone. As the spatial distribution and extent of permafrost directly influences the flow of water through the terrestrial landscape (Sjöberg et al., 2013), adding knowledge about the extent and coverage of permafrost could substantially benefit development of coupled hydrological and carbon transport modeling in northern latitudes (e.g., Jantze et al., 2013; Lyon et al., 2010). This may be particularly important to regions where palsa peatlands make up a large portion of the landscape mosaic and regional-scale differences exist in carbon fluxes (Geisler et al., 2014).

Geophysical methods offer non-intrusive techniques for measuring physical properties of geological materials; however, useful interpretation of geophysical data requires other types of complementary data, such as sediment cores. Ground Penetrating Radar (GPR) has been used extensively in permafrost studies for identifying the boundaries of permafrost (e.g., Arcone et al., 1998; Doolittle et al., 1992; Hinkel et al., 2001; Moorman et al., 2003), characterizing ground ice structures (De Pascale

TCD
8, 5137–5168, 2014

et al., 2008; Hinkel et al., 2001; Moorman et al., 2003), and estimating seasonal thaw depth and moisture content of the active layer (Gacitua et al., 2012; Westermann et al., 2010). Electrical Resistivity Tomography (ERT) has also been widely applied in permafrost studies (Hauck et al., 2003; Ishikawa et al., 2001; Kneisel et al., 2000), the majority of which focus on mountain permafrost. By combining two or more geophysical methods complementary information can often be acquired raising the confidence in interpretations of permafrost characteristics (De Pascale et al., 2008; Hauck et al., 2004; Schwamborn et al., 2002). For example, De Pascale et al. (2008) used GPR and capacitive-coupled resistivity (CCR) to map ground ice in continuous permafrost and demonstrated the added value of combining radar and electrical resistivity measurements for the quality of interpretation of the data. While some non-intrusive geophysical investigations have been done in palsa peatland regions (Dobinski, 2010; Doolittle et al., 1992; Kneisel et al., 2007, 2014; Lewkowicz et al., 2011), the use of multiple geophysical techniques to characterize the extent of permafrost in palsa peatland environments has not been employed.

In this study we use GPR and ERT in concert to map the distribution of permafrost along three transects (160 to 320 m long) in the Tavvavuoma palsa peatland in northern Sweden. Our aim is to understand how depths of the permafrost table surface and base vary in the landscape and, based on resulting estimates of permafrost thickness, to make a first order assessment of the vulnerability of this permafrost to climate warming. Further we hope to demonstrate the added value of employing complimentary geophysical techniques in such landscapes. This novel investigation thus helps contribute to our understanding of the current permafrost distribution and characteristics across palsa peatlands creating a baseline for future studies of possible coupled changes in hydrology and permafrost distribution in such areas.

TCD
8, 5137–5168, 2014

2 Study area

Tavvavuoma is a large palsa peatland complex in northern Sweden at 68°28′ N, 20°54′ E, 550 m a.s.l. (Fig. 1) and is a patchwork of palsas, peat plateaus, thermokarst lakes, hummocks and fens. Ground temperatures and weather parameters have been monitored at the site since 2005 (Christiansen et al., 2010). Sannel and Kuhry (2011) have analyzed lake changes in the area and detailed local studies of palsa morphology have been conducted by Wramner (1968, 1973).

Tavvavuoma is located on a flat valley bottom, in piedmont terrain with relative elevations of surrounding mountains about 50 to 150 m above the valley bottom. Unconsolidated sediments, observed from two borehole cores (points 1 and 2 in Fig. 1), are of mainly glaciofluvial and lacustrine origin and composed of mostly sands, loams and coarser grained rounded gravel and pebbles (Ivanova et al., 2011). The mean annual air temperature is −3.5 °C (Sannel and Kuhry, 2011), and the average winter snow cover in Karesuando, a meteorological station approximately 60 km east of Tavvavuoma, is approximately 50 cm although wind drift generally gives a thinner snow cover in Tavvavuoma (Swedish Meteorological and Hydrological Institute, www.smhi.se/klimatdata/meteorologi).

Permafrost occurs primarily under palsas and peat plateaus in Tavvavuoma, where the average thickness of the active layer is typically 0.5 m (Christiansen et al., 2010; Sannel and Kuhry, 2011). The mean annual temperature in permafrost boreholes (at 2 and 6.1 m depth) in the peatlands of Tavvavuoma range from −0.3 to −0.4 °C (Christiansen et al., 2010). However, no observations of the depth to the permafrost base have been presented for the area. Warming of the air temperature of about 2 °C has been observed in direct measurements from the region over the past 200 years (Klingbjer and Moberg, 2003). In light of this warming, winter precipitation (mainly snow) in northern Sweden shows increasing trends over the past 150 years (Alexandersson, 2002). Further, permafrost is degrading across the region and northern Sweden (Sjöberg et al., 2013). For example, peatland active layer thickness in Abisko (located

TCD
8, 5137–5168, 2014

about 60 km south-west of Tavvavuoma) is increasing according to direct observation over the past 30 years (Åkerman and Johansson, 2008) and inference from hydrologic shifts over the past century (Lyon et al., 2009). This regional permafrost degradation has led to changes in palsas as well. Regionally, reductions in both areas covered by palsas and palsa height have been observed (Sollid and Sorbel, 1998; Zuidhoff, 2002; Zuidhoff and Kolstrup, 2000). In Tavvavuoma, both growth and degradation of palsas have been observed in detailed morphological studies during the 1960's and 1970's (Wramner, 1968, 1973) and expansion and infilling of thermokarstic lakes have been observed through remote sensing analyses (Sannel and Kuhry, 2011). Palsa degradation and infilling of lakes with fen vegetation have been the dominating processes during recent years (Sannel and Kuhry, 2011; Wramner et al., 2012).

3 Theory and methods

Measurements of permafrost extent and structure were made with both GPR and ERT between 20 August 2012 and 26 August 2012 along three transects covering the main permafrost landforms in the Tavvavuoma area (Fig. 1). The ERT transects were somewhat extended (i.e. slight longer) compared to the GPR transects to increase the penetration depth along the overlapping parts of the transects. These summer-time measurements were targeted to capture the potential maximum active layer thicknesses in the region. In addition, GPR measurements were also made along the same transects between 22 March 2012 and 24 March 2012 to explore the winter-time conditions. It was not possible to conduct winter-time measurements with ERT due to large snow coverage and frozen surface conditions.

Transect T1 was 160 m long and crossed a peat plateau that was raised approximately 1.5 m above the surrounding landscape (Fig. 1). It further crossed two thermokarst depressions within the peat plateau. Transect T2 was 320 m long, but the southern part covering about 180 m could not be measured with GPR during the summer campaign due to dense vegetation cover (mainly *salix sp.*). Transect T2 started on

TCD
8, 5137–5168, 2014

a peat plateau surface and continued north over a fen and a small stream. The northern part, measured with both ERT and GPR, crossed a palsa that was raised about 4 m above the surrounding landscape. This palsa has been described via a bore-hole profile (Ivanova et al., 2011, point 1 in Fig. 1). Transect T2 then continued across two fens separated by a lower palsa. Transect T3 was 275 m long. It started on a relatively low palsa and stretched over a flat area covered by hummocks and thermokarst depressions.

In addition to the geophysical investigations (details of which are described in the following sections), the depth to the permafrost table (the active layer) was probed every 2 m along all transects using a 1 m steel rod. Sediment cores were retrieved at four points along T1 and two points along T3 down to 2 m. These cores were used to locate the depth to the peat-mineral substrate interface and the depth to the permafrost table (at points 3, 4, and 5 in Fig. 1). The topography was measured along the transects using a differential GPS with supplemental observations made using an inclinometer where only the ERT was used. The position of the transects was measured using a tape measure and marked at regular intervals to ensure that locations of GPR and ERT transects coincided.

3.1 Ground penetrating radar

Ground penetrating radar (GPR) can be used to map near surface geology and stratigraphy because of differences in dielectric properties between different subsurface layers or structures. An electromagnetic pulse is transmitted through the ground and the return time of the reflected pulse is recorded. The resolution and penetration depth of the radar signal depends on the characteristics of the transmitted pulse and the choice of antennas, which usually range between 10 to 1000 MHz. Higher frequencies will yield a higher resolution but a smaller penetration depth, however, the penetration depth will also depend on dielectric and conductive properties of the ground material. Mapping of permafrost using GPR becomes possible due to the difference in permittivity between unfrozen and frozen water.

TCD
8, 5137–5168, 2014

In this study, GPR measurements were made with 200 MHz antennas on T1 and T2, with the transmitting and receiving antenna held at a constant distance of 0.6 m (common offset). Measurements were made at every 10 cm along the length of these two transects. Along T3 GPR measurement were made using 100 MHz antennas with a 1 m antenna separation and measurements made every 0.2 s while moving the antennas along the transect. The GPR data were processed using a dewow filter, a vertical gain, and a correction for the distance between the transmitting and receiving antennas.

The depth to the permafrost table and the interface between peat-mineral substrates were calculated by converting the two-way travel time to known substrate transitions using estimated velocities for the speed through the different substrate materials. To obtain these substrate velocities, common midpoint (CMP) GPR profiles were measured at two points. These were made by moving the GPR antennae apart from each other in 10 cm increments along the 15 m long transects. The CMP approach, thus, allows for recording the same point in space with different antenna offset making it possible to back out material velocity estimates. The first CMP profile was recorded on a dry peat plateau surface and the second profile on a fully saturated drained lake surface (points 6 and 7 in Fig. 1). These locations were chosen because they are relatively flat and have flat and uniform reflectors making them suitable for CMP measurements. CMP profiles were analysed using semblance analysis in ReflexW software (version 6.1, Sandmeier, 2012, downloaded from www.sandmeier-geo.de).

The speed of the GPR signal was estimated through four different substrates (Table 1). These were, namely, the active layer, talik peat, talik mineral, and frozen ground (see Fig. 2 for conceptual sketch of these substrate layers and velocity profiles). As expected, small scale heterogeneity of these ground materials complicates the interpretation of the CMP results. To account for such uncertainty, in addition to the optimal velocity identified, the maximum and minimum likely velocities for each substrate were considered in the GPR depth conversions. Further, due to inherent difficulties with CMP approaches, unrealistic velocity estimates were complemented with literature defined values for similar substrates.

TCD
8, 5137–5168, 2014

The end product here is a range of plausible substrate velocities accounting for potential uncertainties such that any resultant interpretation about subsurface conditions and interface locations can be considered robust. These are expressed as what can be considered a "representative" velocity bounded by a maximum and a minimum velocity. The active layer velocities were used above the frost table on palsa and peat plateau surfaces that generally consist of relatively dry peat material. For unfrozen peat in fens and under surface depressions where there is a deepening of the permafrost table the talik peat velocities were used. The talik mineral velocities were used for unfrozen mineral sediments, which were assumed to be found only under talik peat. Finally, the velocities for frozen ground were used only when interpreting winter images. Since no local estimates could be made during the winter campaign, literature values for the minimum and maximum velocities were used for interpretations of the GPR data.

3.2 Electrical resistivity tomography

Direct-current electrical resistivity measurements are based on a measured potential difference between two electrodes (ΔV) inserted with galvanic coupling to the ground and, similarly, two electrodes where current is injected into the ground (I) with a known geometric factor (k) depending on the arrangement of the electrodes. This gives a value of the apparent resistivity (ρ_a) of the ground sub-surface as

$$\rho_a = k\Delta V/I. \quad (1)$$

During a tomographic resistivity survey numerous of these measurements are made in both the lateral and vertical (by increasing the electrode spacing). The acquired data is subsequently modeled to generate an image of the resistivity distribution under the site. Values of resistivity vary substantially with grain size, pore size, water content, salinity and temperature (e.g. Reynolds, 2011), thus, the resistivity of permafrost also varies to a large degree. This makes electrical resistivity tomography (ERT) techniques useful in detecting the sharp contrast between frozen and unfrozen water content within sediments.

TCD
8, 5137–5168, 2014

At the Tavvavuoma site, measurements of electrical resistivity were made with electrode spacing of 2 m for the T1 transect and 4 m for the T2 and T3 transects. The Wenner array configuration for the electrodes was used due to its high signal-to-noise ratio and for its accuracy in detecting vertical changes over other common array types (Loke, 2010). For the inversion modeling the smoothness-constrained least-squares method was applied (Loke and Barker, 1996). The inversion progress was set to stop on the condition that the change in root mean squared error from the previous iteration was less than 5 % (implying convergence of the inversion). The software Res2dinv (v.3.59.64) was used for the inversion modeling.

To assess the quality and reliability of the resistivity modeling for the Tavvavuoma site, the depth of investigation (DOI) method (Oldenburg and Li, 1999) was used. This appraisal-technique uses the difference between two inverted models where the reference resistivity parameter is varied to calculate a normalized DOI-index map. From these values a depth at which the surface data is no longer sensitive to the physical properties of the ground can be interpreted. The method has previously been applied in permafrost studies (e.g., Fortier et al., 2008; Marescot et al., 2003). To calculate the DOI-index we used a symmetrical two-sided difference scheme where 0.1 and 10 times the average apparent resistivity of the resistivity model was considered (respectively) for the initial reference resistivity parameter. Normalized DOI values higher than 0.1 indicate that the model is likely not constrained by the data and should be given little significance in subsequent model interpretation.

To further validate the ERT interpretations, one shorter transect with 0.5 m electrode spacing was conducted over a palsa. This was used to acquire local resistivity values for the interface between unfrozen and frozen sediments at the bottom of the active layer (surface of the permafrost table). This value (1700 Ω m) allowed us to map permafrost boundaries in the ERT images. However, as the resistivity of the ground varies with other sediment physical properties and the sediment distribution is complex at the site, the resistivity boundary value for permafrost will naturally vary along transects and with depth. For instance, sands generally have maximum values for the unfrozen state

TCD
8, 5137–5168, 2014

close to 1200 Ω m and for some gravels this can reach up to 3000 Ω m (Hoekstra et al., 1974). Finer sediments, such as clays and silts have lower values, ranging from ca 80 to 300 Ω m (Hoekstra et al., 1974). At our site sands dominate, but there is also evidence of loams. Lewkowicz et al. (2011) report a resistivity of 1000 Ω m at the base of permafrost under a palsa in similar, but somewhat finer, sediments conditions in southern Yukon. This value from Lewkowicz et al. (2011) was thus used as a possible minimum resistivity value for the permafrost boundary in the interpretations, while the local resistivity estimate (1700 Ω m) was used as a maximum and representative value. Again, the motivation here was to account for potential uncertainty allowing for robust interpretation.

3.3 Calculations of active layer and thaw rates

To help put the geophysical measurements and their potential implications for this peatland palsa region in context, the thickness of the active layer as well as first order estimate of long-term thaw rates where estimated using a simple equation for 1-D heat flow by conduction, the Stefan equation (as described by Riseborough et al., 2008):

$$Z = \sqrt{\frac{2\lambda I}{L n}}, \tag{2}$$

where Z is the thaw depth, λ is thermal conductivity, I is the thawing degree day index (as described by Nelson and Outcalt, 1987), L is the volumetric latent heat of fusion and n is the saturated porosity of the ground substrate. As a talik is by definition unfrozen ground occurring in a permafrost area, the Eq. (2) was used to confirm that the ground identified as talik in Tavvvavuoma through the GPR and ERT images did not correspond to locations of thicker active layer relative to surrounding positions (i.e. provide a confirmation that these sites would not freeze during winter).

Calculations of active layer thickness in fens were made using as input a sinusoidal annual air temperature curve generated from the average temperature of the warmest and the coldest months of the year. The effect of the snow cover, which would give

TCD
8, 5137–5168, 2014

higher ground surface temperatures in the winter, was not explicitly taken into consideration in this simple calculation as we did not have any direct estimates of snow cover available for the transects. As such, these calculations are simply a first-order approximation. Representative properties for saturated peat where chosen, including a thermal conductivity of 0.5 $W m^{-1} K^{-1}$ and a saturated fraction of 0.80 (Woo, 2012).

In addition, a first-order approximation of long-term thaw rates was carried out as a thought experiment. An instantaneous increase in air temperature of 2 °C was assumed, which represents a warming within current climate projections for the 21st century, although at the low end of projections for Arctic warming (IPCC RA5, 2013). A thermal conductivity of 3 $W m^{-1} K^{-1}$ and a saturated fraction of 0.50 were used to represent a sand soil, slightly oversaturated with ice. The annual freezing degree days were subtracted from the annual thawing degree days, I in Eq. (2), and the amount of days necessary to thaw the estimated local thickness of permafrost was estimated. This is a simple estimate since, clearly, the Stefan equation is not designed to calculate long-term thaw rates nor does such an estimate consider any density dependent feedbacks and/or subsequent hydroclimatic shifts. Regardless, combined with estimates of permafrost thickness made in our geophysical investigation, the aim of this thought experiment was to provide an order-of-magnitude estimate for the time it could potentially take permafrost to completely thaw out at this site to help place it in a pan-arctic context.

4 Results

4.1 GPR data

In the summer GPR images the permafrost table was clearly detectable under the palsa and peat plateau surfaces along all transects (Fig. 3). The interface between peat and mineral substrates was only detectable in unfrozen sediments. Deeper reflections, interpreted as the permafrost table under supra-permafrost taliks, were found under

TCD
8, 5137–5168, 2014

the fens and surface depression in all transect. In the beginning of both transects T1 and T2, deep reflections that end abruptly were present in the images at about 250 and 150 ns, respectively. In T1, this corresponds to a wet fen bordering a lake and for T2 it corresponds to a fen bordering a stream. The proximity to these water bodies suggests that these are likely not reflections from the permafrost table. The base of the permafrost could not be detected at any point in the GPR images likely because of loss of signal strength at depth.

In the winter GPR images, interfaces between frozen and unfrozen ground (taliks) were not clearly separable from sedimentary layers. Several interfaces are visible in the images, however, indicating a complex layering of sediments and ground ice confirmed by described sedimentary profiles from the site (Ivanova et al., 2011). No further interpretations were made from winter images, however, due to the lack of clear reflections.

4.2 ERT data

The results from the ERT data modelling showed areas of high resistivity (1000–100 000 Ω m) where permafrost could be expected due to the sharp contrast to surrounding surfaces. This suggests permafrost boundaries are detectable for both the extent of the horizontal distribution and the vertical extent to the base of permafrost (Fig. 4). The highest resistivity values were found under the peat plateau in T1 and under the palsas in T2 and T3. Low resistivity values were found under the fens in all transects. DOI values increase with depth for all transects allowing the permafrost base to be interpreted only along parts of T2. Counter to this, under T1 and T3 the DOI rapidly increases under the peat plateau and hummocks. Due to the wide electrode spacing adopted (2 and 4 m), the permafrost table under the active layer is too shallow to be visible in the ERT data.

TCD
8, 5137–5168, 2014

4.3 Geophysical interpretations

Permafrost occurs under the palsa and peat plateau surfaces along T1 and T2, as well as under the hummocks along T3 (Fig. 5). The active layer depths estimated from the GPR data closely matched the depths measured in the field (Table 2). This is expected since measured active layer depths along T1 and T2 were used to derive the velocity of the radar signal in the active layer. The depth to the base of the permafrost could only be estimated with good confidence along parts of T2 and is on average 15.8 m from the ground surface and at least 25 m at its deepest point. Along transects T1 and T3 the deepest permafrost was found at 8.4 and 23.4 m respectively; however, the permafrost base could not be identified with confidence below this depth.

Potential taliks (Table 3 and Fig. 5) are numerous and occur in both wet fens, such as all taliks along T2, and relatively dry depressions in the terrain, such as all taliks along T1. The sediment cores used for estimating the GPR representative signal velocity in talik peat were taken in both a relatively dry location and in a wet fen, but the calculated velocities were nearly identical, indicating that the soil moisture at depth was similar at both locations. Most of T3 was underlain by taliks and these were found under both wet fens and drier surface depressions. The taliks range in depth from 2.1 m (T3f, numbering from Table 3 and Fig. 5) to 6.7 m (T1c) based on the GPR data and are slightly deeper based on the ERT results. From the ERT data, T1c is in fact interpreted as a potential through-going talik. Talik T1b was only detected from the ERT data, and taliks T3b–T3d appear as one large talik in the ERT data.

4.4 Calculations of active layer and thaw rates

The active layer depths calculated using the Stefan equation support the interpretation that identified taliks do not freeze during winter. The seasonal frost penetration depth was estimated to be 0.72 m which is about the same as the average peat depth along the transects and much less than the estimated minimum depth of the taliks (2.1 m). While a shallower peat depth would give a deeper frost penetration it is unlikely that

TCD
8, 5137–5168, 2014

the seasonal frost penetration is > 2.1 m in the area surrounding Tavvavuoma. This ancillary estimate confirms the aforementioned geophysical interpretation. Further, as a thought experiment, assuming a 2 °C instantaneous temperature increase at the site, the long-term thaw rate was calculated to be 7 cm year^{-1}. At this rate, the time to completely thaw out permafrost assuming the estimated average thickness along T2 (15.3 m) was calculated to be 175 years.

5 Discussion

5.1 Permafrost and talik distribution at Tavvavuoma

The spatial pattern of permafrost and taliks in Tavvavuoma is closely linked to the distribution of palsas, peat plateaus, fens and water bodies. This suggests that local factors, such as soil moisture, groundwater flow, ground ice content, sediment distributions and geomorphology, strongly influence the local ground thermal regime (see e.g. Delisle and Allard, 2003; McKenzie and Voss, 2013; Woo, 2012; Zuidhoff, 2002). The relative elevation of permafrost landforms, as well as permafrost resistivity values and sediment distributions suggest that there is a large variation in ground ice content in the area. Surface elevations of palsas and peat plateaus are highest along T2 and lowest along T3, indicating a higher ice content of the underlying ground along T2, which is likely related to differences in ground substrates between the transects. Coring (< 2 m) across the site, as well as existing borehole descriptions (Ivanova et al., 2011) confirm that the ground contains a larger fraction of coarse glaciofluvial sand and gravel, which are not susceptible to frost heave, closer to T3 as compared to T2.

Lewkowicz et al. (2011) used the height of palsas and permafrost thickness, estimated by ERT, to calculate excess ice fractions (EIF) in permafrost mounds in southern Yukon. For Tavvavuoma, the EIF at the top of the highest palsa at T2 was 0.25, which is comparable to those reported by Lewkowicz et al. (2011), which were generally ranging between 0.2 and 0.4. For T3 possible maximum EIFs were calculated

TCD
8, 5137–5168, 2014

using the greatest depths at which permafrost was found, since the permafrost base could not be identified from the data for T3. The calculated EIFs along T3 were on average < 0.03 and at maximum < 0.09, confirming that ground ice content is lower along this transect. The relatively low resistivity of the permafrost along T3 further supports interpretations for lower ice content in this permafrost. Permafrost with low ice content is more susceptible to thaw, as less energy is needed for latent heat exchange. This provides a possible explanation for why taliks are more widespread along T3, as permafrost with a low ice content would have reacted more rapidly to warming in the area.

The calculated thaw rate of $7\,\mathrm{cm\,year^{-1}}$ is considerably higher than the circa $1\,\mathrm{cm\,year^{-1}}$ deepening of the active layer observed in the region (Åkerman and Johansson, 2008) and inferred from hydrological records (Lyon et al., 2009). One possible reason for this is that these observations were made in the relatively ice rich top layer of peat, while for the calculations in this study a medium with higher thermal conductivity and lower ice content was used to represent the lower mineral sediment layer. The $2\,^{\circ}\mathrm{C}$ instantaneous step change in temperature could further have contributed to the higher thaw rates compared to the ones observed. As thawing is driven by gradients in heat it can be argued that permafrost thaw rates should increase with warmer air temperatures. Considering this, the calculated time of complete permafrost thaw out of about 175 years can be considered reasonable in at least an order of magnitude. However, much more rapid palsa degradation has been observed in the region (Zuidhoff, 2002), due to block and wind erosion processes and thermal influence on palsas from expanding water bodies, and very rapid decay of palsa surface areas has been observed in both southern Norway and the Canadian Arctic (Payette et al., 2004; Sollid and Sorbel, 1998). The coupled erosion, hydrological and thermal processes are not represented in the Stefan equation but can be of great importance for permafrost thaw rates (McKenzie and Voss, 2013; Painter et al., 2013; Zuidhoff, 2002). There is clearly a need for quantification of the relative importance of these processes for permafrost thaw to better understand expected future changes in these environments.

TCD
8, 5137–5168, 2014

5.2 On the complementary nature of the geophysical techniques

Several previous studies have shown the benefits of combining more than one geophysical technique for mapping permafrost (e.g. De Pascale et al., 2008; Hauck et al., 2004; Schwamborn et al., 2002), and also in this study the GPR and ERT data provided complementary information that allowed for interpretations that would not have been possible by using only one of the two datasets. Of course, combining multiple techniques for inference compounds our estimate uncertainties. To attain more precise estimates of depths to the different interfaces, deeper coring data would have been necessary for both more accurate signal velocity estimates for the GPR and for local resistivity values of the ground materials. The fact that ERT depth estimates are consistently higher than the GPR estimates suggest that either the resistivity boundary value for permafrost is in fact lower than our local estimate, or that GPR signal velocities are higher than the values used in this study. Since our local permafrost resistivity estimate was made in peat at the permafrost table, which can have a very high ice content compared to deeper sediment layers, it is a more likely explanation for this discrepancy.

GPR and ERT yielded somewhat overlapping data but the two datasets have different strengths and therefore complement each other well. The GPR data worked well for identifying the permafrost table with high confidence, especially in the top 2 m where sediment cores could be easily obtained for validation and signal velocity estimates. This suitability of GPR for identifying permafrost interfaces in the top 1–2 m has been shown in several studies (e.g. Doolittle et al., 1992; Hinkel et al., 2001; Moorman et al., 2003). GPR was however not a suitable technique for detecting the permafrost base during winter, due to the high variability in ground ice content and sediment layering in this environment. The ERT data, using the setup in this study, does not yield data in the uppermost part of the ground and also has higher uncertainty where resistivity contrasts are high (Fig. 4), which makes it less well suited for the active layer and shallow taliks. With the ERT data it is, however, possible to image relatively deep in the ground, where the GPR cannot penetrate. By combining both GPR and ERT the active

TCD
8, 5137–5168, 2014

layer, the base of permafrost, and potential taliks could be identified along at least parts of the transects, which could not have been achieved with good confidence by either of the two methods alone.

6 Concluding remarks

Peat plateau complexes offer an interesting challenge to the Cryosphere community as they are clear mosaics combining local-scale differences manifested as permafrost variations. As such variation occurs both horizontally and vertically in the landscape, geophysical techniques offer a good possibility to record current permafrost conditions across scales. Complementary methods, such as GPR and ERT as demonstrated here, are necessary as they can provide orthogonal views of the permafrost extents. The results of this study show a heterogeneous pattern of permafrost extent reflecting both local and climatic processes of permafrost formation and degradation. To improve our understanding of landscape-permafrost interactions and dynamics will require a community effort to benchmark variability across the scales and environments within the pan-arctic. This is particularly important in lesser studied regions and across the sporadic permafrost zone where changes are occurring rapidly.

Author contributions. Ylva Sjöberg designed the study, carried out the GPR measurements and analysis, and did the main writing of the manuscript. Per Marklund carried out the ERT measurements and analysis and did the main writing for the sections on ERT methods and ERT results, as well as commented on the whole manuscript. Rickard Pettersson provided input on the geophysical techniques and analyses and commented on the whole manuscript. Steve Lyon provided input on the project design and commented on the whole manuscript, including language and style.

Acknowledgements. This study was kindly supported by Sveriges Geologiska Undersökning (SGU), The Bolin Centre for Climate Research, Lagrelius fond, Göran Gustafssons Stiftelse för natur och miljö i Lappland, and Svenska Sällskapet för Antropologi och Geografi. The authors are grateful to Peter Jansson and Britta Sannel for lending us the equipment necessary for this

TCD
8, 5137–5168, 2014

study, and to Romain Pannetier, Kilian Krüger, Matthias Siewert, Britta Sannel, and Lars Labba for fieldwork support. We are also grateful to Andrew Parsekian for technical advice on the GPR survey design and María A. García Juanatey for assistance in processing the ERT data.

References

Åkerman, H. J. and Johansson, M.: Thawing permafrost and thicker active layers in sub-arctic Sweden, Permafrost Periglac., 19, 279–292, doi:10.1002/ppp.626, 2008.

Alexandersson, H.: Temperature and precipitation in Sweden 1860–2001, SMHI, Norrköping, Sweden, 2002.

Arcone, S. A., Lawson, D. E., Delaney, A. J., Strasser, J. C., and Strasser, J. D.: Ground-penetrating radar reflection profiling of groundwater and bedrock in an area of discontinuous permafrost, Geophysics, 63, 1573–1584, doi:10.1190/1.1444454, 1998.

Christiansen, H. H., Etzelmuller, B., Isaksen, K., Juliussen, H., Farbrot, H., Humlum, O., Johansson, M., Ingeman-Nielsen, T., Kristensen, L., Hjort, J., Holmlund, P., Sannel, A. B. K., Sigsgaard, C., Akerman, H. J., Foged, N., Blikra, L. H., Pernosky, M. A., and Odegard, R. S.: The Thermal State of Permafrost in the Nordic Area during the International Polar Year 2007–2009, Permafrost Periglac., 21, 156–181, doi:10.1002/ppp.687, 2010.

Davis, J. L. and Annan, A. P.: Ground-penetrating radar for high-resolution mapping of soil and rock, Geophys. Prospect., 37, 531–551, doi:10.1111/j.1365-2478.1989.tb02221.x, 1989.

De Pascale, G. P., Pollard, W. H., and Williams, K. K.: Geophysical mapping of ground ice using a combination of capacitive coupled resistivity and ground-penetrating radar, Northwest Territories, Canada, J. Geophys. Res.-Earth, 113, F02S90, doi:10.1029/2006jf000585, 2008.

Delisle, G. and Allard, M.: Numerical simulation of the temperature field of a palsa reveals strong influence of convective heat transport by groundwater, Permafrost, Proceeding of the 8th International Permafrost Conference, Zurich, Switzerland, 21–25 July 2003, 181–186, 2003.

Dobinski, W.: Geophysical characteristics of permafrost in the Abisko area, northern Sweden, Pol. Polar Res., 31, 141–158, doi:10.4202/ppres.2010.08, 2010.

Doolittle, J. A., Hardisky, M. A., and Black, S.: A ground-penetrating radar study of Goodstream palsas, Newfoundland, Canada, Arctic Alpine Res., 24, 173–178, doi:10.2307/1551537, 1992.

Evans, S.: Dielectric properties of ice and snow – a review, J. Glaciol., 5, 20, 773–792, 1965.

TCD
8, 5137–5168, 2014

Fortier, R., LeBlanc, A. M., Allard, M., Buteau, S., and Calmels, F.: Internal structure and conditions of permafrost mounds at Umiujaq in Nunavik, Canada, inferred from field investigation and electrical resistivity tomography, Can. J. Earth Sci., 45, 367–387, doi:10.1139/e08-004, 2008.

Gacitua, G., Tamstorf, M. P., Kristiansen, S. M., and Uribe, J. A.: Estimations of moisture content in the active layer in an Arctic ecosystem by using ground-penetrating radar profiling, J. Appl. Geophys., 79, 100–106, doi:10.1016/j.jappgeo.2011.12.003, 2012.

Giesler, R., Lyon, S. W., Mörth, C.-M., Karlsson, J., Karlsson, E. M., Jantze, E. J., Destouni, G., and Humborg, C.: Catchment-scale dissolved carbon concentrations and export estimates across six subarctic streams in northern Sweden, Biogeosciences, 11, 525–537, doi:10.5194/bg-11-525-2014, 2014.

Hauck, C., Vonder Muhll, D., and Maurer, H.: Using DC resistivity tomography to detect and characterize mountain permafrost, Geophys. Prospect., 51, 273–284, doi:10.1046/j.1365-2478.2003.00375.x, 2003.

Hauck, C., Isaksen, K., Muhll, D. V., and Sollid, J. L.: Geophysical surveys designed to delineate the altitudinal limit of mountain permafrost: an example from Jotunheimen, Norway, Permafrost Periglac., 15, 191–205, doi:10.1002/ppp.493, 2004.

Hinkel, K. M., Doolittle, J. A., Bockheim, J. G., Nelson, F. E., Paetzold, R., Kimble, J. M., and Travis, R.: Detection of subsurface permafrost features with ground-penetrating radar, Barrow, Alaska, Permafrost Periglac., 12, 179–190, doi:10.1002/ppp.369, 2001.

Hoekstra, P., Selimann, P., and Delaney, A.: Airborne resistivity mapping of permafrost near Fairbanks, Alaska, US Army CRREL, Hanover, New Hampshire, 51, 1974.

Hugelius, G., Bockheim, J. G., Camill, P., Elberling, B., Grosse, G., Harden, J. W., Johnson, K., Jorgenson, T., Koven, C. D., Kuhry, P., Michaelson, G., Mishra, U., Palmtag, J., Ping, C.-L., O'Donnell, J., Schirrmeister, L., Schuur, E. A. G., Sheng, Y., Smith, L. C., Strauss, J., and Yu, Z.: A new data set for estimating organic carbon storage to 3 m depth in soils of the northern circumpolar permafrost region, Earth Syst. Sci. Data, 5, 393–402, doi:10.5194/essd-5-393-2013, 2013.

Hugelius, G., Strauss, J., Zubrzycki, S., Harden, J. W., Schuur, E. A. G., Ping, C. L., Schirrmeister, L., Grosse, G., Michaelson, G. J., Koven, C. D., O'Donnell, J. A., Elberling, B., Mishra, U., Camill, P., Yu, Z., Palmtag, J., and Kuhry, P.: Improved estimates show large circumpolar stocks of permafrost carbon while quantifying substantial uncertainty ranges and identifying

TCD
8, 5137–5168, 2014

remaining data gaps, Biogeosciences Discuss., 11, 4771–4822, doi:10.5194/bgd-11-4771-2014, 2014.
IPCC: Climate Change 2013: The Physical Science Basis, Contribution of Working Group I to the Fifth Assessment Report of the Intergovernmental Panel on Climate Change, edited by: Stocker, T. F., Qin, D., Plattner, G.-K., Tignor, M., Allen, S. K., Boschung, J., Nauels, A., Xia, Y., Bex, V., and Midgley, P. M., Cambridge University Press, Cambridge, UK and New York, NY, USA, 1535 pp., 2013.
Ishikawa, M., Watanabe, T., and Nakamura, N.: Genetic differences of rock glaciers and the discontinuous mountain permafrost zone in Kanchanjunga Himal, eastern Nepal, Permafrost Periglac., 12, 243–253, doi:10.1002/ppp.394, 2001.
Ivanova, N. V., Kuznetsova, I. L., Parmuzin, I. S., Rivkin, F. M., and Sorokovikov, V. A.: Geocryological Conditions in Swedish Lapland, Proceedings of the 4th Russian Conference on Geocryology, Moscow State University, Russia, 7–9 June 2011, 77–82, 2011.
Jantze, E. J., Lyon, S. W., and Destouni, G.: Subsurface release and transport of dissolved carbon in a discontinuous permafrost region, Hydrol. Earth Syst. Sc., 17, 3827–3839, doi:10.5194/hess-17-3827-2013, 2013.
Joseph, S., Giménez, D., and Hoffman, J. L.: Dielectric permittivity as a function of water content for selected New Jersey soils, New Jersey Geological and Water Survey, Trenton NJ, available at: http://www.state.nj.us/dep/njgs/geodata/dgs10-1.htm (last access: 17 December 2013), 2010.
Klingbjer, P. and Moberg, A.: A composite monthly temperature record from Tornedalen in northern Sweden, 1802–2002, Int. J. Climatol., 23, 1465–1494, doi:10.1002/joc.946, 2003.
Kneisel, C., Hauck, C., and Vonder Muhll, D.: Permafrost below the timberline confirmed and characterized by geoelectrical resistivity measurements, Bever Valley, eastern Swiss Alps, Permafrost Periglac., 11, 295–304, doi:10.1002/1099-1530(200012)11:4<295::AID-PPP353>3.0.CO;2-L, 2000.
Kneisel, C., Saemundsson, D., Beylich, A. A.: Reconnaissance surveys of contemporary permafrost environments in central Iceland using geoelectrical methods: implications for permafrost degradation and sediment fluxes, Geogr. Ann. A, 89, 41–50, doi:10.1111/j.1468-0459.2007.00306.x, 2007.
Kneisel, C., Emmert, A., Kästl, J.: Application of 3D electrical resistivity imaging for mapping frozen ground conditions exemplified by three case studies, Geomorphology, 210, 71–82, doi:10.1016/j.geomorph.2013.12.022, 2014.

TCD
8, 5137–5168, 2014

Lewkowicz, A. G., Etzelmuller, B., and Smith, S. L.: Characteristics of Discontinuous Permafrost based on Ground Temperature Measurements and Electrical Resistivity Tomography, Southern Yukon, Canada, Permafrost Periglac., 22, 320–342, doi:10.1002/ppp.703, 2011.
Loke, M. H.: Rapid 2-D Resistivity & IP inversion using the least-squares method (RES2DINV ver. 3.59 for Windows XP/Vista/7, manual), Geotomo Software, Malaysia, 2010.
Loke, M. H. and Barker, R. D.: Rapid least-squares inversion of apparent resistivity pseudosections by a quasi-Newton method, Geophys. Prospect., 44, 131–152, doi:10.1111/j.1365-2478.1996.tb00142.x, 1996.
Lyon, S. W., Destouni, G., Giesler, R., Humborg, C., Mörth, M., Seibert, J., Karlsson, J., and Troch, P. A.: Estimation of permafrost thawing rates in a sub-arctic catchment using recession flow analysis, Hydrol. Earth Syst. Sci., 13, 595–604, doi:10.5194/hess-13-595-2009, 2009.
Lyon, S. W., Mörth, M., Humborg, C., Giesler, R., and Destouni, G.: The relationship between subsurface hydrology and dissolved carbon fluxes for a sub-arctic catchment, Hydrol. Earth Syst. Sc., 14, 941–950, doi:10.5194/hess-14-941-2010, 2010.
Marescot, L., Loke, M. H., Chapellier, D., Delaloye, R., Lambiel, C., and Reynard, E.: Assessing reliability of 2D resistivity imaging in mountain permafrost studies using the depth of investigation index method, Near Surf. Geophys., 1, 57–67, 2003.
McKenzie, J. M. and Voss, C. I.: Permafrost thaw in a nested groundwater-flow system, Hydrogeol. J., 21, 299–316, doi:10.1007/s10040-012-0942-3, 2013.
Moorman, B. J., Robinson, S. D., and Burgess, M. M.: Imaging periglacial conditions with ground-penetrating radar, Permafrost Periglac., 14, 319–329, doi:10.1002/ppp.463, 2003.
Nelson, F. E. and Outcalt, S. I.: A computational method for prediction and regionalization of permafrost, Arctic Alpine Res., 19, 279–288, doi:10.2307/1551363, 1987.
Oldenburg, D. W. and Li, Y. G.: Estimating depth of investigation in dc resistivity and IP surveys, Geophysics, 64, 403–416, doi:10.1190/1.1444545, 1999.
Painter, S. L., Moulton, J. D., Wilson, C. J.: Modeling challenges for predicting hydrologic response to degrading permafrost, Hydrogeol. J., 21, 221–224, doi:10.1007/s10040-012-0917-4, 2013.
Payette, S., Delwaide, A., Caccianiga, M., Beauchemin, M.: Accelerated thawing of subarctic peatland permafrost over the last 50 years, Geophys. Res. Lett., 31, L18208, doi:10.1029/2004GL020358, 2004.
Reynolds, J. M.: An Introduction to Applied and Environmental Geophysics, 2 Ed., John Wiley & Sons, Hoboken, 2011.

TCD
8, 5137–5168, 2014

Riseborough, D., Shiklomanov, N., Etzelmuller, B., Gruber, S., and Marchenko, S.: Recent advances in permafrost modelling, Permafrost Periglac., 19, 137–156, doi:10.1002/ppp.615, 2008.
Sannel, A. B. K. and Kuhry, P.: Warming-induced destabilization of peat plateau/thermokarst lake complexes, J. Geophys. Res.-Biogeo., 116, G03035, doi:10.1029/2010jg001635, 2011.
Schwamborn, G. J., Dix, J. K., Bull, J. M., and Rachold, V.: High-resolution seismic and ground penetrating radar-geophysical profiling of a thermokarst lake in the western Lena Delta, northern Siberia, Permafrost Periglac., 13, 259–269, doi:10.1002/ppp.430, 2002.
Seppälä, M.: Synthesis of studies of palsa formation underlining the importance of local environmental and physical characteristics, Quaternary Res., 75, 366–370, doi:10.1016/j.yqres.2010.09.007, 2011.
Sollid, J. L. and Sorbel, L.: Palsa bogs as a climate indicator – examples from Dovrefjell, southern Norway, AMBIO, 27, 287–291, 1998.
Sjöberg, Y., Frampton, A., and Lyon, S. W.: Using streamflow characteristics to explore permafrost thawing in northern Swedish catchments, Hydrogeol. J., 21, 121–131, doi:10.1007/s10040-012-0932-5, 2013.
Tarnocai, C., Canadell, J., Mazhitova, G., Schuur, E. A. G., Kuhry, P., and Zimov, S.: Soil organic carbon stocks in the northern circumpolar permafrost region, Global Biogeochem. Cy., 23, GB2023, doi:10.1029/2008GB003327, 2009.
Westermann, S., Wollschläger, U., and Boike, J.: Monitoring of active layer dynamics at a permafrost site on Svalbard using multi-channel ground-penetrating radar, The Cryosphere, 4, 475–487, doi:10.5194/tc-4-475-2010, 2010.
Woo, M.-K.: Permafrost Hydrology, Springer, Heidelberg, 563 pp., 2012.
Wramner, P.: Studier av palsmyrar i Tavvavuoma och Laivadalen, Lappland (Studies of palsa mires in Tavvavuoma and Laivadalen, Lappland), Licenciate Thesis, Göteborg University, Gothenburg, Sweden, 1968.
Wramner, P.: Palsmyrar i Tavvavuoma, Lappland (Palsa mires in Tavvavuoma, Lapland), GUNI report 3, Göteborg University, Gothenburg, Sweden, 1973.
Wramner, P., Backe, S., Wester, K., Hedvall, T., Gunnarsson, U., Alsam, S., and Eide, W.: Förslag till övervakningsprogram för Sveriges palsmyrar (Proposed monitoring program for Sweden's palsa mires), Länsstyrelsen i Norrbottens Län, Luleå, Sweden, 2012.

TCD
8, 5137–5168, 2014

Zuidhoff, F. S.: Recent decay of a single palsa in relation to weather conditions between 1996 and 2000 in Laivadalen, northern Sweden, Geogr. Ann. A, 84, 103–111, doi:10.1111/1468-0459.00164, 2002.

Zuidhoff, F. S. and Kolstrup, E.: Changes in palsa distribution in relation to climate change in Laivadalen, northern Sweden, especially 1960–1997, Permafrost Periglac., 11, 55–69, doi:10.1002/(SICI)1099-1530(200001/03)11:1<55::AID-PPP338>3.0.CO;2-T, 2000.

TCD
8, 5137–5168, 2014

Table 1. Velocities used for converting two-way travel times to depth in GPR data.

Material	Velocity ($m\,ns^{-1}$)	Method/source
Active layer – representative	0.049	Calibration against every second field measurements* of active layer depths
Active layer – min	0.046	Representative estimate minus one SD of field measurements[a]
Active layer – max	0.052	Representative estimate plus one SD of field measurements[a]
Talik peat – representative	0.036	Calibration against coring (point 3 and 5, in Fig. 1)
Talik peat – min	0.033	Velocity in pure water (Davis and Annan, 1989)
Talik peat – max	0.049	Representative estimate for active layer peat
Talik mineral – representative	0.060	Velocity in sand and clay from Davis and Annan (1989)
Talik mineral – min	0.053	Calculated minimum from Joseph et al. (2010) for saturated loams and sands
Talik mineral – max	0.073	Highest estimated velocity from CMP analysis
Frozen ground – min	0.110	Minimum for permafrost from Hinkel et al. (2001)
Frozen ground – max	0.160	Velocity in pure ice from Evans (1965)

[a] Field measurement using a 1 m steel rod.

TCD
8, 5137–5168, 2014

Table 2. Range of interpreted depths (m) of active layer, peat-mineral interface, and permafrost base averaged along transects at Tavvavuoma.

	T1			T2			T3		
	Min[a]	Representative[b]	Max[c]	Min[a]	Representative[b]	Max[c]	Min[a]	Representative[b]	Max[c]
Active layer									
Observed[d]		0.51			0.52			0.56	
GPR	0.50	0.53	0.57	0.48	0.51	0.54	0.52	0.56	0.59
Peat-mineral interface									
GPR	0.77	0.84	1.14	0.68	0.74	1.01	0.63	0.69	0.93
Permafrost base									
ERT		–	–		15.8	17.3		–	–

[a] GPR: using the estimated minimum velocity (Table 1). ERT: using 1000 Ω m resistivity boundary (talik);
[b] GPR: using representative estimate velocity (Table 1). ERT: using 1700 Ω m resistivity value;
[c] GPR: using the estimated maximum velocity (Table 1). ERT using 1000 Ω m resistivity boundary (permafrost base);
[d] Depth from manual field measurement using a steel probe.

TCD
8, 5137–5168, 2014

Table 3. Estimated depths (m) of taliks. Numbering is the same as in Fig. 5.

Talik max depth	GPR min[a]	GPR representative[b]	GPR max[c]	ERT min[a]	ERT representative[b]
T1a	2.4	2.7	3.4	2.5	3.1
T1b	–	–	–	1.6	2.8
T1c	6.0	6.7	8.3	> 4.7	> 4.7
T2a	5.4	6.1	7.6	5.4	6.9
T2b	5.3	6.0	7.4	6.9	8.8
T3a	5.3	5.9	7.4	5.8	7.8
T3b	5.7	6.4	8.0	6.3	8.2
T3c	5.1	5.7	7.0	4.8	7.9
T3d	3.1	3.5	4.4	–	4.0
T3e	4.6	5.2	6.4	5.4	7.2
T3f	2.0	2.1	2.2	–	3.8
T3g	3.7	4.1	5.2	5.0	6.8

[a] GPR: using the estimated minimum velocity (Table 1). ERT: using 1000 Ω m resistivity boundary (talik);
[b] GPR: using representative estimate velocity (Table 1). ERT: using 1700 Ω m resistivity value;
[c] GPR: using the estimated maximum velocity (Table 1). ERT using 1000 Ω m resistivity boundary (permafrost base).

TCD
8, 5137–5168, 2014

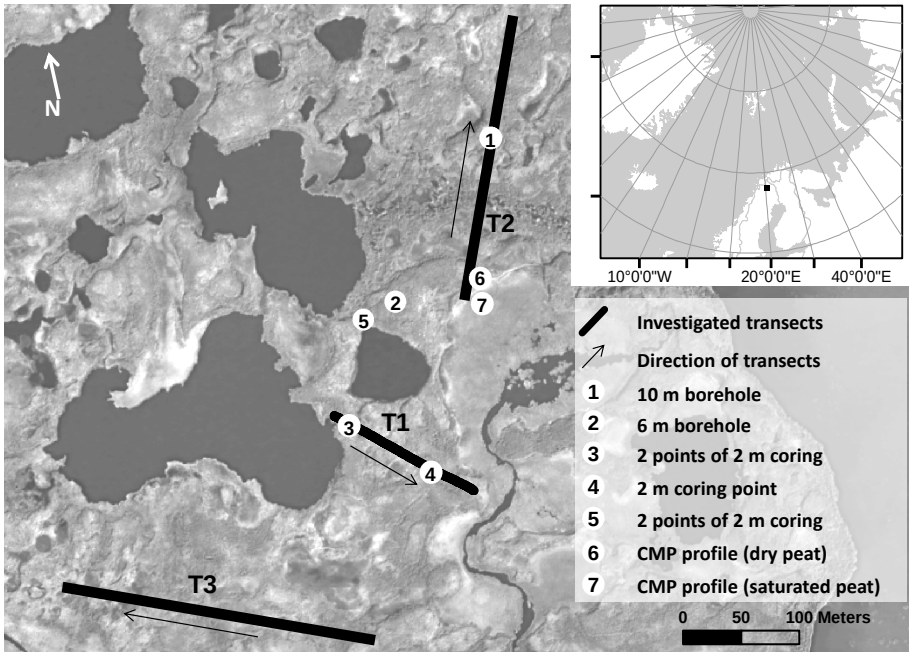

Figure 1. Location of the study site (inset), investigated transects, existing boreholes (Ivanova et al., 2011, points 1 and 2), coring points, and points of CMP measurements (described in Sect. 3.1). (Aerial photograph from Lantmäteriet, the Swedish land survey, 2012.)

TCD
8, 5137–5168, 2014

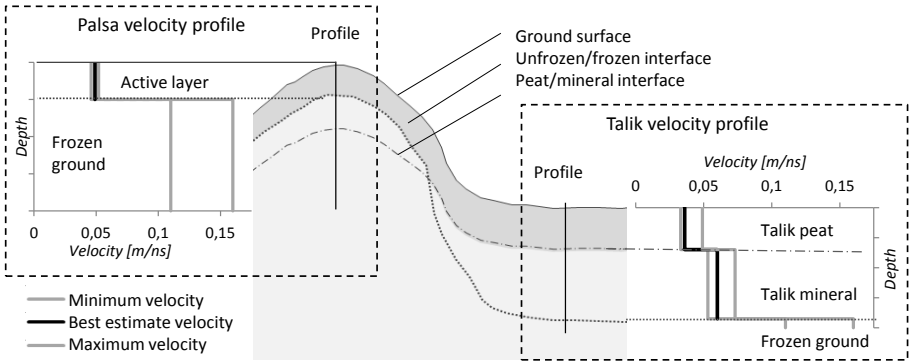

Figure 2. Conceptual sketch of typical distribution of ground substrates and associated estimated velocities for a palsa and talik ground profile.

TCD
8, 5137–5168, 2014

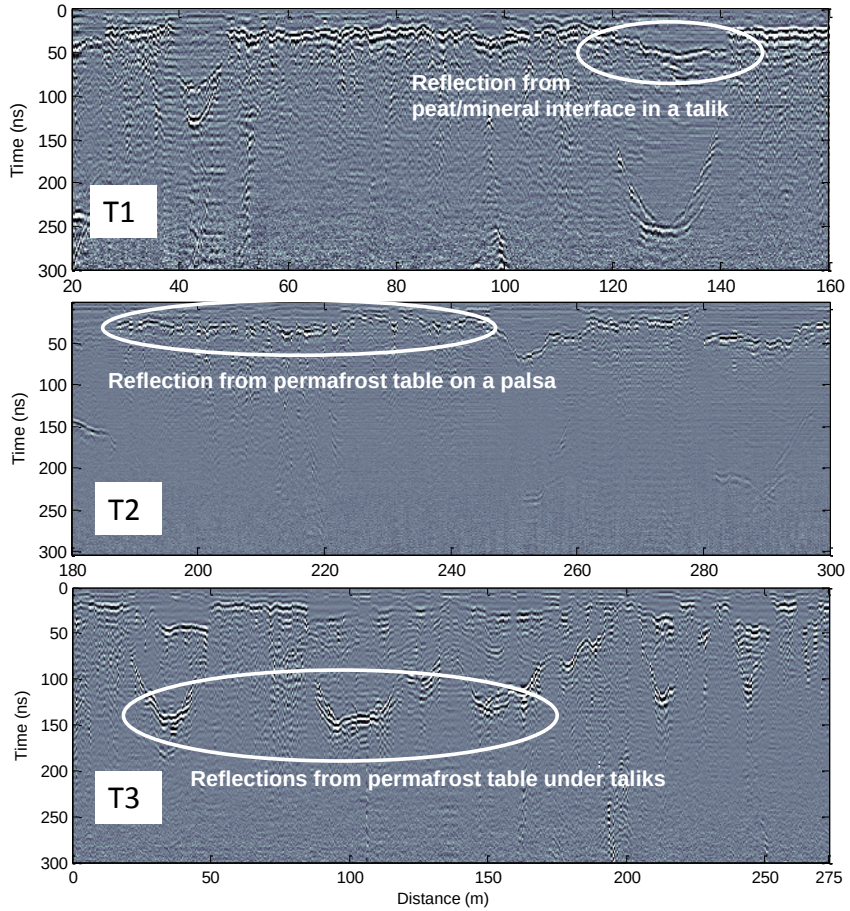

Figure 3. GPR images for T1, T2, and T3 with selected reflections marked as examples of interfaces that were identified for this study.

TCD
8, 5137–5168, 2014

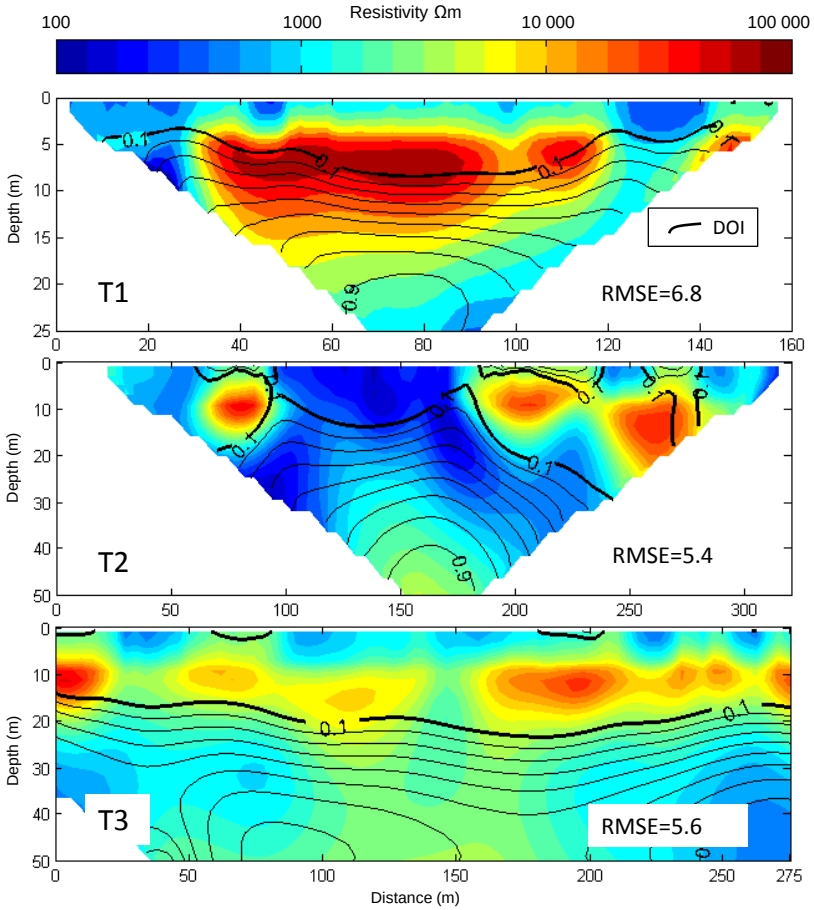

Figure 4. ERT results for T1, T2, and T3. DOI > 0.1 (black lines) indicates that the model is well constrained by the data.

TCD
8, 5137–5168, 2014

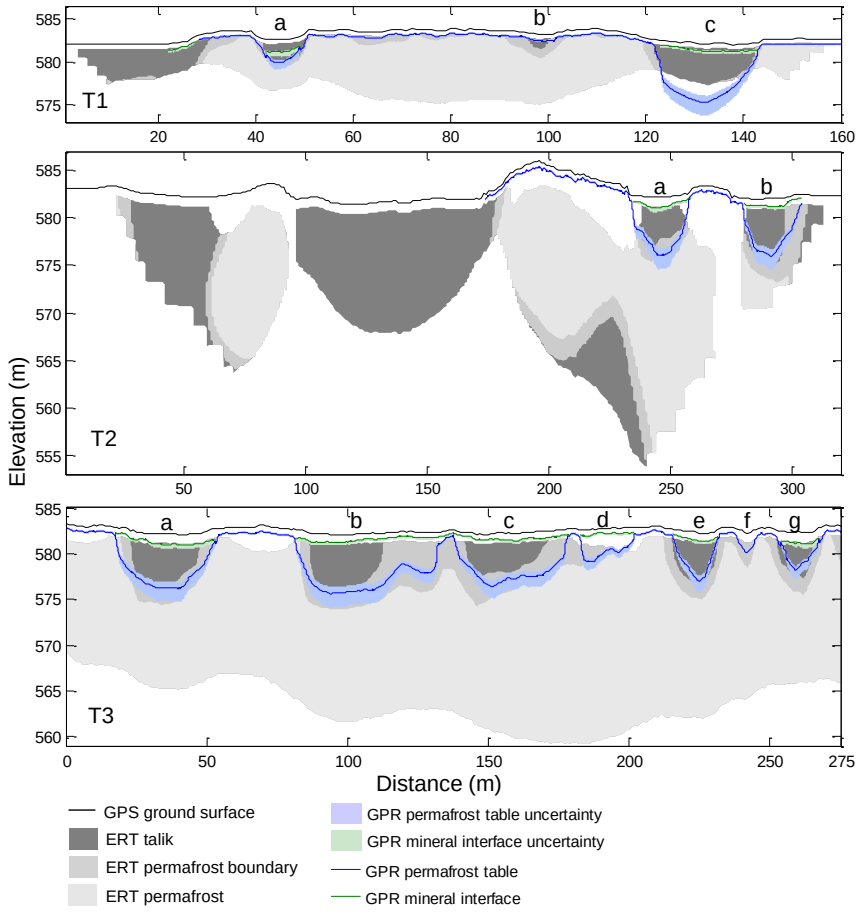

Figure 5. Interpreted permafrost distribution along T1, T2, and T3. Note the differences in scale in the x-direction between figures and the vertical exaggeration.

TCD
8, 5137–5168, 2014